Huurdeman, E.P., et al., 2020, Rapid expansion of meso-megathermal rain forests into the southern high latitudes at the onset of the Paleocene-Eocene Thermal Maximum: Geology, v. 48, https://doi.org/10.1130/G47343.1

Table DR1. Table showing the fossil pollen and spore taxa encountered in the Point Margaret section, their nearest living relatives, and supporting references. Taxa are listed in alphabetical order. Relictual taxa and cosmopolitan taxa within the nearest living relatives are marked by (*) and (**), respectively. References are given below the table.

Taxon	Nearest Living Relative	Reference
Araucariacites australis	Araucariaceae; *Araucaria, Agathis*	1
Arecipites spp.	Arecaceae	1
Australopollis obscurus	Callitrichaceae; *Callitriche***	4, 10
Baculatisporites spp.	Osmundaceae	1
Banksieaeidites arcuatus	Proteaceae; *Musgravea*	1
Bluffopollis scabratus	Strasburgeriaceae; *Strasburgeria**	1, 8
Casuarinidites cainozoicus	Casuarinaceae; *Gymnostoma*	1, 4
Ceratosporites equalis	Lycopodiaceae, Selaginellaceae; *Selaginella***	1, 10
Clavatipollenites glarius	Chloranthaceae; *Ascarina*	4
Clavifera triplex	Gleicheniaceae	1
Crassoretitriletes vanraadshoovenii	Schizaeaceae; *Lygodium*	4
Cyathides australis	Cyatheaceae	1
Cycadopites spp.	*Cycadophyta/Ginkgophyta*	11
Dacrycarpites australiensis	Podocarpaceae; *Dacrycarpus*	1
Dictyophyllidites arcuatus	Gleicheniaceae, *Dicranopteris*	1
Dilwynites granulatus	Araucariaceae; *Wollemia/Agathis*	1, 2
Dilwynites tuberculatus	Araucariaceae; *Wollemia/Agathis*	1, 3
Dryptopollenites semilunatus	Pandanaceae; *Freycinetia*	1, 4
Ericipites scabratus	Ericaceae; Styphelоideae	4
Gleicheniidites circinidites/senonicus	Gleicheniaceae	1
Haloragacidites harrisii	Casuarinaceae; *Gymnostoma*	1, 4
Lygistepollenites florinii	Podocarpaceae; *Dacrydium*	4
Malvacipollis diversus/subtilis	*Austrobuxus, Dissiliaria, Petalostigma*	1, 11
Microachryidites antarcticus	Podocarpaceae; *Microstrobos, Microcachrys**	1, 4
Nothofagidites brachyspinulos	*Nothofagus* (subg. *Fuscospora*)*	4
Nothofagidites emarcidus	*Nothofagus* (subg. *Brassospora*)	4
Nothofagidites flemingii	*Nothofagus* (subg. N*othofagus*)*	4
Nyssapollenites cf. *N. endobalteus*	Euphorbiaceae; *Macaranga, Mallotus*	1, 11, 13
Osmundacidites spp.	Osmundaceae	1
Parvisaccites catastus	Podocarpaceae; *Halocarpus**	1, 4
Periporopollenites demarcatus	Trimeniaceae; *Trimenia*	1, 4
Periporopollenites polyporatus	Trimeniaceae; *Trimenia*	1, 4

Phyllocladidites mawsonii	Podocarpaceae; *Lagarostrobos**	1, 4
Podocarpidites ellipticus	Podocarpaceae; *Podocarpus*	1
Polypodiaceoisporites retirugatus	Pteridaceae; *Pteris*	4
Polypodiisporites cf. *inangahuensis*	Polypodiaceae; *Davallia*	1
Polypodiisporites speciosus	Polypodiaceae	11
Propylipollis annularis	Proteaceae; *Xylomelum occidentale*	1, 4
Proteacidites adenonthoides	Proteaceae; *Adenanthos**	1, 10
Proteacidites crassus	Proteaceae; possibly *Adenanthos**	1, 5
Proteacidites latrobensis	Proteaceae; cf. *Megahertzia**	1, 7
Proteacidites pseudomoides	Proteaceae; *Carnarvonia/Lomatia*	1, 7, 10
Proteacidites reticuloscabratus	Proteaceae; *Gevuina/Hicksbeachia*	1
Proteacidites spp.	Proteaceae	1
Retitriletes austroclavatidites	Lycopodiaceae; *Lycopodium***	1
Spinizonocolpites prominatus	Arecaceae; *Nypa*	4
Stereisporites maastrichtiensis	Sphagnaceae; *Sphagnum***	4
Tricolpites reticulatus	Gunneraceae; *Gunnera*	1, 6
Triporopollenites ambiguus	Proteaceae; *Telopea/Oreocallis*	1

References for Nearest Living Relatives:

1. Raine, J.I., Mildenhall, D.C., and Kennedy, E.M., 2011, New Zealand fossil spores and pollen: an illustrated catalogue, 4th edition, GNS Science Miscellaneous Series No. 4, http://data.gns.cri.nz/sporepollen/index.htm
2. Macphail, M.K., and Carpenter, R.J., 2014, New potential nearest living relatives for Araucariaceae producing fossil Wollemi Pine-type pollen (*Dilwynites granulatus* WK Harris, 1965): Alcheringa, v. 38, p. 135-139, https://doi.org/10.1080/03115518.2014.843145.
3. Macphail, M.K., Carpenter, R.J., Iglesias, A., and Wilf, P., 2013, First evidence for Wollemi pine-type pollen (*Dilwynites*: Araucariaceae) in South America: PloS one, v. 8, e69281, https://doi.org/10.1371/journal.pone.0069281.
4. Macphail, M.K., Alley, N.F., Truswell, E.M., and Sluiter, I.R.K., 1994, Early Tertiary vegetation: evidence from spores and pollen, *in* Hill, R.S., ed., History of the Australian vegetation: Cretaceous to recent: Cambridge University Press, p. 189-261, https://doi.org/10.20851/australian-vegetation.
5. Cookson, I.C., 1950, Fossil pollen grains of Proteaceous type from Tertiary deposits in Australia: Australian Journal of Science, series B, v. 3, p. 166-177, https://doi.org/10.1071/BI9500166.
6. Wanntorp, L., Dettmann, M.E., and Jarzen, D.M., 2004, Tracking the Mesozoic distribution of *Gunnera*: comparison with the fossil pollen species *Tricolpites reticulatus* Cookson: Review of Palaeobotany and Palynology, v. 132, p. 163-174, https://doi.org/10.1016/j.revpalbo.2004.06.001.
7. Macphail, M.K., 1999, Palynostratigraphy of the Murray Basin, inland southeastern Australia: Palynology, v. 23, p. 197-240, https://doi.org/10.1080/01916122.1999.9989528.
8. Jarzen, D.M., and Pocknall, D.T., 1993, Tertiary *Bluffopollis scabratus* (Couper) Pocknall & Mildenhall, 1984 and modern *Strasburgeria* pollen: a botanical comparison: New Zealand Journal of Botany, v. 31, p. 185-192, https://doi.org/10.1080/0028825X.1993.10419493.

9. Gee, C.T., 2001, The mangrove palm *Nypa* in the geologic past of the New World: Wetlands Ecology and Management, v. 9, p. 181-203, https://doi.org/10.1023/A:1011148522181.
10. Dettmann, M.E., 1994, Cretaceous vegetation: the microfossil record. in Hill, R.S., ed., History of the Australian vegetation: Cretaceous to recent: Cambridge University Press, p. 143-170, https://doi.org/10.1071/BT18143.
11. Martin, H.A. 1974, The identification of some Tertiary pollen belonging to the family Euphorbiaceae. Australian Journal of Botany, v. 22, p. 271-29, https://doi.org/10.1071/BT9740271
12. Carpenter, R.J., Macphail, M.K., Jordan, G.J., and Hill, R.S., 2015, Fossil evidence for open, Proteaceae-dominated heathlands and fire in the Late Cretaceous of Australia: American Journal of Botany, v. 102, p. 2092-2107, https://doi.org/10.3732/ajb.1500343.
13. Lee, D.E., Bannister, J.M., Raine, J.I., and Conran, J.G., 2010, Euphorbiaceae: Acalyphoideae fossils from early Miocene New Zealand: *Mallotus–Macaranga* leaves, fruits, and inflorescence with in situ *Nyssapollenites endobalteus* pollen: Review of Palaeobotany and Palynology, v. 163, p. 127-138, https://doi.org/10.1016/j.revpalbo.2010.10.002.

Table DR2. Climatic requirements of the nearest living relatives used in the pollen- and spore-based temperature estimates for the Point Margaret section. Nearest living relatives are listed in alphabetical order. Relictual taxa (*) and cosmopolitan taxa (**) were excluded from the analysis. MAAT = mean annual air temperature; SD = standard deviation. Modern distribution refers to the DOI that links to the modern distribution of the nearest living relative in the GBIF database (gbif.org).

Nearest Living Relative	MAAT	SD	Modern distribution
*Adenanthos**	16.1	2.6	10.15468/dl.xc1ha5
Anacolosa/Cathedra	25.3	2	10.15468/dl.pqlknu
Araceae/Amaryllidaceae**	10.9	5	10.15468/dl.tfehqb
Araucaria+Agathis	19.2	4	10.15468/dl.q69bzn
Arecaceae	22.4	4.4	10.15468/dl.wc9h3c
Ascarina	13.7	4.8	10.15468/dl.eispu7
Austrobuxus/Dissiliaria/Petalostigma	25	3.2	10.15468/dl.fqeqza
Brassospora	18.2	3.9	10.15468/dl.4wafw1
*Callitriche**	7.9	3.3	10.15468/dl.g9hphy
Cyatheaceae	14.7	5.2	10.15468/dl.rnaahg
Cycadales	20.7	4.4	10.15468/dl.5u19gi
Dacrycarpus	13.5	4.4	10.15468/dl.oy4lkz
Dacrydium	12.5	4.9	10.15468/dl.7yiqqq
Davallia	19.2	4.6	10.15468/dl.du12oe
Dicranopteris	21.8	4.4	10.15468/dl.xtwwir
Dryopteridaceae	10.4	5.2	10.15468/dl.rjkyth
Freycinetia	17	5.9	10.15468/dl.cxq0vz

*Fuscospora**	8.7	4.1	10.15468/dl.x6zd6s
Gevuina/Hicksbeachia	18.3	4.1	10.15468/dl.j4lyef
Gleicheniaceae	16.8	5.4	10.15468/dl.xtwwir]
Gunnera	12.2	4.4	10.15468/dl.87dbkb
Gymnostoma	23.4	2.8	10.15468/dl.cutuoy
*Halocarpus**	8.9	4.3	10.15468/dl.potfwl
Ilex	17.3	5.7	10.15468/dl.yrr0ec
*Lagarostrobos+Manoao**	10.9	2.7	10.15468/dl.5jdsci
*Laurelia**	12.2	2.4	10.15468/dl.opprxx
Lomatia+Carnarvonia	14.1	3.3	10.15468/dl.vovepn
*Lycopodium***	6.3	4.2	10.15468/dl.jk7nr3
Lygodium	22.8	4.4	10.15468/dl.fia0r5
Mallotus+Macaranga	22.9	4.1	10.15468/dl.cl6rgv
Megahertzia	24.6	0.9	10.15468/dl.po2a5x
Metrosideros	11.8	4	10.15468/dl.v2hsfh
*Microcachrys/Pherosphaera**	7.7	5.2	10.15468/dl.cazawk
Musgravea/Austromuellera	22.5	2	10.15468/dl.in9tb7
*Nothofagus**	6.9	4.9	10.15468/dl.hhhvww
Nypoideae	26.1	2	10.15468/dl.wc9h3c
Osmundaceae	10.6	3.4	10.15468/dl.8xsj6w
Podocarpus	13.3	5.6	10.15468/dl.jl31ua
Polypodiaceae	11.7	5.8	10.15468/dl.gesnzu
Proteaceae	18	4.8	10.15468/dl.z7gsmv
Pteris	18.3	4.5	10.15468/dl.kkbbu1
*Selaginella***	9.6	8.7	10.15468/dl.kzpmmj
*Sphagnum***	6.1	3.6	10.15468/dl.zdcjyp
*Strasburgeria**	20.2	2.6	10.15468/dl.c8qzxn
Styphelioideae	14.4	2.9	10.15468/dl.iayg2n
Telopea/Oreocallis	12.2	3.7	10.15468/dl.ah44a5
Trimenia	16.2	3.1	10.15468/dl.3yzfo7
Wollemia/Agathis	18.6	4.5	10.15468/dl.belkxz
Xylomelum	16.9	2.4	10.15468/dl.wemcqh

Text DR1:

BrGDGT sourcing and validity assessment

Branched glycerol dialkyl glycerol tetraether (brGDGT) based proxies can be sensitive to alternate sourcing, especially in shallow-marine settings (e.g., Sinninghe Damste, 2016), where *in situ* produced or riverine brGDGTs may alter the initial soil or peat derived distributions. Significant non-soil contributions may prohibit the use of standard modern calibration datasets, but these contributions are readily identified by comparing the recorded brGDGT distributions to the global modern soil and peat databases (De Jonge et

al., 2014a; Naafs et al., 2017b). We find that the brGDGT distributions at Point Margaret plot with the modern soils or peats (Figure DR1). Furthermore, the penta- and hexa-methylated isomerization ratios (IR; De Jonge et al., 2014b) indicating potential riverine brGDGT contributions are generally very low (<0.4). Also the weighed number of rings in the tetra- and penta-methylated brGDGTs is <0.4, where values >0.7 suggest a marine source (Sinninghe Damsté, 2016), consistent with brGDGT distributions in modern low-pH tropical soils. Indeed, when compared to other Paleogene brGDGT data, our data appears to be similar to the Paleogene lignites (e.g., Naafs et al., 2018; Hollis et al., 2019). As we find no indication for significant contributions of non-soil-derived brGDGTs, we here use the transfer function of Naafs et al. (2017a) to convert MBT'_{5me} values to Mean Annual Air Temperature (MAAT) estimates.

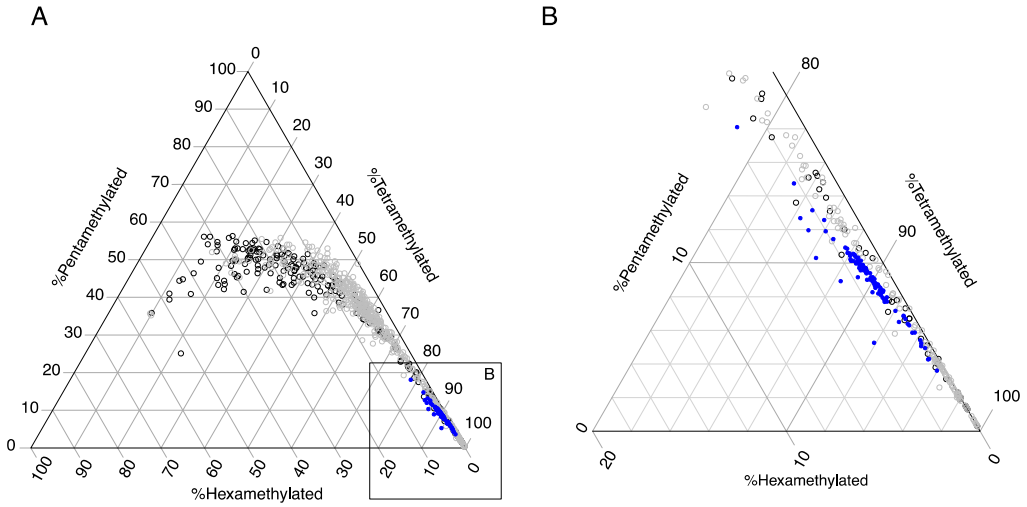

Figure DR1. Ternary plot showing the %tetra-, penta- and hexa-methylated brGDGTs in the Point Margaret samples (blue dots), compared to modern soils (De Jonge et al., 2014a) (black circles) and modern peats (Naafs et al., 2017b) (gray circles). The box in panel A indicates the enlarged area shown in panel B.

References for BrGDGT sourcing and validity assessment:

De Jonge, C., Hopmans, E.C., Zell, C.I., Kim, J.H., Schouten, S., and Sinninghe Damsté, J.S., 2014a, Occurrence and abundance of 6-methyl branched glycerol dialkyl glycerol tetraethers in soils: Implications for palaeoclimate reconstruction: Geochimica et Cosmochimica Acta, v. 141, p. 97-112, https://doi.org/10.1016/j.gca.2014.06.013.

De Jonge, C., Stadnitskaia, A., Hopmans, E.C., Cherkashov, G., Fedotov, A., and Sinninghe Damsté, J.S., 2014b, In situ produced branched glycerol dialkyl glycerol tetraethers in suspended particulate matter from the Yenisei River, Eastern Siberia: Geochimica et Cosmochimica Acta, v. 125, p. 476-491, https://doi.org/10.1016/j.gca.2013.10.031.

Hollis, C.J., et al., 2019, The DeepMIP contribution to PMIP4: methodologies for selection, compilation and analysis of latest Paleocene and early Eocene climate proxy data,

incorporating version 0.1 of the DeepMIP database: Geoscientific Model Development Discussions 2019, p. 1-98, https://doi.org/10.5194/gmd-2018-309.
Naafs, B.D.A., Gallego-Sala, A.V., Inglis, G.N., and Pancost, R.D., 2017a, Refining the global branched glycerol dialkyl glycerol tetraether (brGDGT) soil temperature calibration: Organic Geochemistry, v. 106, p. 48-56, https://doi.org/10.1016/j.orggeochem.2017.01.009.
Naafs, B.D.A., et al., 2017b, Introducing global peat-specific temperature and pH calibrations based on brGDGT bacterial lipids: Geochimica et Cosmochimica Acta, v. 208, p. 285-301, https://doi.org/10.1016/j.gca.2017.01.038.
Naafs, B.D.A., et al., 2018, High temperatures in the terrestrial mid-latitudes during the early Palaeogene: Nature Geoscience, v. 11, p. 766, https://doi.org/10.1038/s41561-018-0199-0.
Sinninghe Damsté, J.S., 2016, Spatial heterogeneity of sources of branched tetraethers in shelf systems: The geochemistry of tetraethers in the Berau River delta (Kalimantan, Indonesia): Geochimica et Cosmochimica Acta, v. 186, p. 13-31, https://doi.org/10.1016/j.gca.2016.04.033.

Text DR2:
Timing of individual proxy signals

The null hypothesis that the warming is recorded synchronously between all MAT proxies and synchronous with the observed CIE was tested using cross-correlation functions (CCFs). The analyses conducted here are primarily designed to identify and quantify the stratigraphic offset between the various carrier signals across the PETM CIE (here: $\delta^{13}C$, brGDGTs, and pollen assemblages). The approach is very similar to that of Frieling et al. (2019), but focuses on the depth domain, which can be converted into approximate temporal offsets with the use of average accumulation rates.

We focused on a 3-m-thick stratigraphic interval that encompasses the CIE onset and the intervals directly above and below (49.3–52.3 m). The brGDGT and pollen data were resampled to the approximate average stratigraphic resolution of the $\delta^{13}C$ curve, with an equally spaced sample resolution of 5 cm. The data were not detrended in order to focus entirely on the relative positions of the shift in the various proxy carriers rather than any background variability. Perhaps with the exception of the vegetation-based proxies, all signals can be assumed principally independent signal recorders. There are no indications that the bulk organic matter sourcing changed dramatically across the CIE (Frieling et al., 2018), precluding large offsets in either stratigraphic position or magnitude that have been identified elsewhere (e.g., Sluijs et al., 2012; Sluijs and Dickens, 2012).

The background noise in the data remains well below <25% of the total signal across the CIE, which is a signal-noise level previously found to yield an acceptable number of false positives (e.g., Frieling et al., 2019). The stratigraphic offsets using our CCFs are small (i.e., on the order of 0–20 cm) and confirm our visual inspection. The largest offset

(15–20 cm) is found between $\delta^{13}C$ and brGDGTs, where the observed brGDGT response lags that in $\delta^{13}C$ (Fig. 4). The $\delta^{13}C$ signal also leads the variable "%mega-mesothermal elements" by c. 10 cm, but the $\delta^{13}C$ signal lags the NLR signal by 5–10cm. The CCF analyses show warming in the NLR MAAT data as a small lead (5–10cm) to the $\delta^{13}C$ curve, but the magnitude of this offset is dampened relative to the positions where the first signs of warming in vegetation (appearance of *Nypa* at 50.57 m) and $\delta^{13}C$ change (50.8 m) are observed. This is because the CCF analyses rely on the averaged response across the dataset. As the NLR-derived MAAT stabilizes and even briefly decreases again during the CIE onset, this pushes the average response towards zero, despite the stratigraphic lead (c. 25 cm) of the first warming signals. These effects are not obvious in the other, smoother, MAAT reconstructions. The first rise in NLR MAAT can hence be interpreted as evidence for 'pre-CIE' warming, while the CCFs detect potentially millennial-scale offsets in proxy carriers due to various carrier-specific mechanisms described below.

The delay in the variables "brGDGTs" and "%meso-megathermal elements" is not necessarily representative of true delayed warming. In contrast, the delay in "%meso-megathermal" can be explained by the presence of a fern spike at the start of the CIE (Fig. 2), likely representing a period where soils were disturbed. As a consequence, a slight delay in establishing the meso-megathermal vegetation is expected, both because of the closed-sum effect and the actual delay in colonization. Indeed, when the CCFs are conducted with the relative abundance of ferns added to meso-megathermal vegetation to reflect the main vegetation overhaul, the signal becomes synchronous with the CIE.

Following this line of reasoning, it is expected that soil organic matter (brGDGTs) was eroded in greater quantity from pre-CIE deposits during the intervals with disturbed vegetation cover. Aging of terrestrial organic matter can be on the order of several kys in the sub- modern realm (Schefuß et al., 2016), and enhanced erosion is documented repeatedly for the PETM CIE (e.g., John et al., 2012; Sluijs et al., 2014), including clay-bound organic matter (Schneider-Mor and Bowen, 2013). In this context, it is noteworthy that pollen and brGDGTs represent different sources within the terrestrial realm, with associated different transport mechanisms, and that signals derived from, e.g., pollen and BIT often broadly match qualitatively, but rarely quantitatively in geological records (e.g., Sluijs et al., 2011).

The delay between the $\delta^{13}C$ signal and wide establishment of meso-megathermal elements is hence interpreted as the combined result of vegetation disturbance and colonization time. Likewise, it is reasonable to assume that enhanced soil erosion delivered pre-aged organic matter including brGDGTs during the initial phase of the PETM, but given evidence on the composition of the organic matter (Frieling et al., 2018), it is unlikely that

soil organic matter contributes significantly to the total organic matter in these sediments at any point.

References for timing of individual proxy signals:

Frieling, J., Huurdeman, E.P., Rem, C.C.M., Donders, T.H., Pross, J., Bohaty, S.M., Holdgate, G.R., Gallagher, S.J., McGowran, B., and Bijl, P.K., 2018, Identification of the Paleocene-Eocene boundary in coastal strata in the Otway Basin, Victoria, Australia: Journal of Micropalaeontology, v. 37, p. 317-339.

Frieling, J., Peterse, F., Lunt, D.J., Bohaty, S.M., Damsté, J.S.S., Reichart, G.J., and Sluijs, A., 2019, Widespread warming before and elevated barium burial during the Paleocene-Eocene Thermal Maximum: evidence for methane hydrate release?: Paleoceanography and Paleoclimatology, v. 34, p. 546-566.

John, C.M., Banerjee, N.R., Longstaffe, F.J., Sica, C., Law, K.R., and Zachos, J.C., 2012, Clay assemblage and oxygen isotopic constraints on the weathering response to the Paleocene-Eocene thermal maximum, east coast of North America: Geology, v. 40, p. 591-594.

Schefuß, E., Eglinton, T.I., Spencer-Jones, C.L., Rullkötter, J., De Pol-Holz, R., Talbot, H.M., Grootes, P.M., and Schneider, R.R., 2016, Hydrologic control of carbon cycling and aged carbon discharge in the Congo River basin: Nature Geoscience, v. 9, p. 687-690.

Schneider□Mor, A., and Bowen, G.J., 2013, Coupled and decoupled responses of continental and marine organic□sedimentary systems through the Paleocene□Eocene thermal maximum, New Jersey margin, USA : Paleoceanography, v. 28, p.105-115.

Sluijs, A., Bijl, P.K., Schouten, S., Röhl, U., Reichart, G.J., and Brinkhuis, H., 2011, Southern ocean warming, sea level and hydrological change during the Paleocene-Eocene thermal maximum: Climate of the Past, v. 7, p. 47-61.

Sluijs, A., Zachos, J.C., and Zeebe, R.E., 2012, Constraints on hyperthermals: Nature Geoscience, v. 5, p. 231-231.

Sluijs, A., and Dickens, G.R., 2012, Assessing offsets between the δ13C of sedimentary components and the global exogenic carbon pool across early Paleogene carbon cycle perturbations: Global Biogeochemical Cycles, v. 26, https://doi.org/10.1029/2011GB004224.

Sluijs, A., Van Roij, L., Harrington, G.J., Schouten, S., Sessa, J.A., LeVay, L.J., Reichart, G.J., and Slomp, C.P., 2014, Warming, euxinia and sea level rise during the Paleocene–Eocene Thermal Maximum on the Gulf Coastal Plain: implications for ocean oxygenation and nutrient cycling: Climate of the Past, v. 10, p. 1421-1439.

Figures DR2 and DR3. Photographs of selected sporomorphs of the Point Margaret section in alphabetical order. Scale bars equal 20 µm.

Figure DR2 – Plate 1

a. *Arecipites* spp. *(*Arecaceae*)* #35 23-24 slide 1 EFC: Q34-2

b. *Bluffopollis scabratus (*Strasburgeriaceae*)* #34 20-21 slide 1 EFC: T19-2

c. *Crassoretitriletes vanraadshoovenii (Lygodium)* #34 20-21 slide 1 EFC: U32-1

d. *Cyathidites* spp. *(*Cyatheaceae*)* PP333 slide 1 EFC: T26-2

e. *Dictyophyllidites arcuatus (*Gleicheniaceae*)* PP361 slide 1 EFC: L17-2

f. *Dilwynites granulatus (Agathis/Araucaria)* PP25 slide 1 EFC: K25-2

g. *Ericipites scabratus (*Stypheloideae*)* PP355 slide 1 EFC: U37-4

h. *Gleicheniidites senonicus* (Gleicheniaceae*)* #33 22-23 slide 1 EFC :O21-2

i. *Haloragacidites harrisii (Gymnostoma)* #34 46.5-48 slide 1 EFC: N26-3

j. *Laevigatosporites ovatus* (Filiicopsida) #33 22-33 slide 1 EFC: H16-2 H16-4

k. *Lygistepollenites florinii (Dacrydium)* PP166 slide 2 EFC: P36-1

l. *Malvacipollis diversus (Austrobuxus)* #34 46.5-48 slide 1 EFC: L32

m. *Microachryidites antarcticus (Microachrys)* PP181 slide 1 EFC: X28-2 X28-4

n. *Nyssapollenites* cf. *N. endobalteus (Macaranga/Mallotus)* #35 33-34 slide 1 EFC: K37-4

o. *Nyssapollenites* cf. *N. endobalteus (Macaranga/Mallotus)* #35 33-34 slide 1 EFC: E20-1

Figure DR3 – Plate 2

a. *Parvisaccites catastus* (*Halocarpus*) PP25 slide 1 EFC: S30-3 T30-1

b. *Phyllocladidites mawsonii* (*Lagorostrobos*) PP181 slide 1 EFC: P35-2 P34-4

c. *Podocarpidites ellipticus* (*Podocarpus*) PP25 slide 1 EFC: U34-2

d *Periporopollenites demarcatus* (*Trimenia*) PP355 slide 1 EFC: Q32-3

e *Periporopollenites polyoratus* (*Trimenia*) PP181 slide 1 EFC: Q29-2

f. *Polypodiaceoisporites retirugatus* (*Pteris*) #34 46.5-48 slide 1 EFC: S19-4/T19-2

g. *Proteacidites adenanthoides* (*Adenanthos*) PP355 slide 1 EFC: S30-1

h. *Proteacidites annularis* (*Xylomelum*) PP181 slide 1 EFC: R26-4

i. *Proteacidites pachypolus* (extinct Proteaceae) #34 10-11 slide 1 EFC: G32-3

j. *Spinizonicolpites prominatus* (*Nypa*) #34 39 40 slide 1 EFC: G29-1

k. *Spinizonicolpites prominatus* (*Nypa*) PP361 slide 1 EFC: H19-1

l. *Todisporites minor* (Osmundaceae) #34 20-21 slide 1 EFC: D31-3

m. *Todisporites minor* (Osmundaceae) PP 361 slide 1 EFC: K34-1

n. *Tripunctisporites maastrichtiensis* (*Sphagnum*) PP223 slide 1 EFC: H36-1/H36-2

o. *Tricolporites microreticulatus* (unknown affinity) #34 46.5-48 slide 1 EFC: M32-

Plate 1

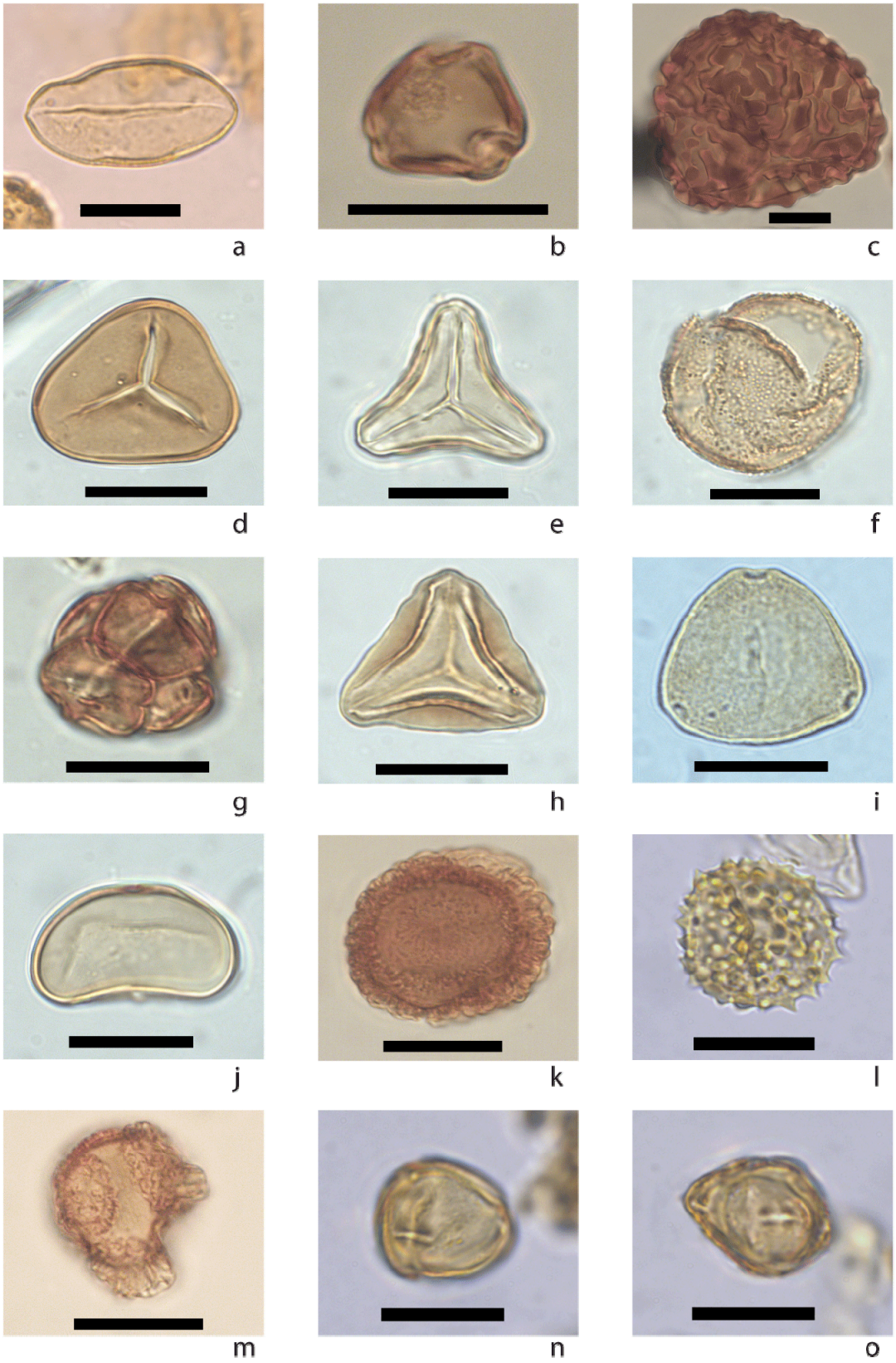

Plate 2